

Is Registering Raw Tagged-MR Enough for Strain Estimation in the Era of Deep Learning?

Zhangxing Bian^a, Ahmed Alshareef^b, Shuwen Wei^a, Junyu Chen^a, Yuli Wang^a, Jonghye Woo^c, Dzung L. Pham^d, Jiachen Zhuo^e, Aaron Carass^a, and Jerry L. Prince^a

^aJohns Hopkins University, Baltimore MD, US

^bUniversity of South Carolina, Columbia SC, US

^cMassachusetts General Hospital and Harvard Medical School, Boston MA, US

^dUniformed Services University of the Health Sciences, Bethesda MD, US

^eUniversity of Maryland School of Medicine, Baltimore MD, US

ABSTRACT

Magnetic Resonance Imaging with tagging (tMRI) has long been utilized for quantifying tissue motion and strain during deformation. However, a phenomenon known as tag fading, a gradual decrease in tag visibility over time, often complicates post-processing. The first contribution of this study is to model tag fading by considering the *interplay* between T_1 relaxation and the repeated application of radio frequency (RF) pulses during serial imaging sequences. This is a factor that has been overlooked in prior research on tMRI post-processing. Further, we have observed an emerging trend of utilizing *raw* tagged MRI within a deep learning-based (DL) registration framework for motion estimation. In this work, we evaluate and analyze the impact of commonly used image similarity objectives in training DL registrations on *raw* tMRI. This is then compared with the Harmonic Phase-based approach, a traditional approach which is claimed to be robust to tag fading. Our findings, derived from both simulated images and an actual phantom scan, reveal the limitations of various similarity losses in raw tMRI and emphasize caution in registration tasks where image intensity changes over time.

Keywords: MR tagging, deep learning registration, image similarity, strain estimation

1. INTRODUCTION

Tagged Magnetic Resonance Imaging (tMRI) ^{1,2} is a technique that has been employed for numerous years to visualize and quantify the intricate movements of tissues undergoing deformation. ³⁻⁵ This technique is used in many applications including assessing myocardial function, ^{6,7} studying motion during speech and swallowing, ^{4,8-10} and measuring brain motion after low-acceleration impacts. ⁵ MR tagging temporarily magnetizes tissue with a spatially modulated periodic pattern, creating transient tags in the image sequence that move with the tissue, thus capturing motion and strain information.

Processing tMRI must contend with the phenomenon of tag fading, characterized by a gradual decrease in tag visibility over time. The cause of tag fading is traditionally ascribed to T_1 relaxation. In the present study, we delve deeper into the modelling of tag fading, considering the *interplay* between T_1 relaxation and the repeated application of radio frequency (RF) pulses during serial image acquisition. This understanding is important because the fading pattern of tags substantially influences subsequent estimations of motion and strain. Algorithms like optical flow and image registration are often used to track tag motion across time frames. ¹¹⁻¹⁶ However, the fading of tags disrupts the premise of brightness constancy, which in turn hampers tracking and yields less precise estimates of tissue motion.

The Harmonic Phase (HARP) method is a widely recognized approach for processing tMRI and is reported to exhibit robustness against tag fading. ^{11,17,18} HARP applies a bandpass filter on harmonic peaks in k -space to obtain the harmonic phase, which is assumed to be an innate, spatially-varying property of the material being imaged. HARP-based tracking approaches ^{12,13,19} employ harmonic phase images in the registration framework for motion tracking, and thus should not be influenced by the brightness changes induced by tag fading.

Further author information: (Send correspondence to Zhangxing Bian: zbian4@jhu.edu)

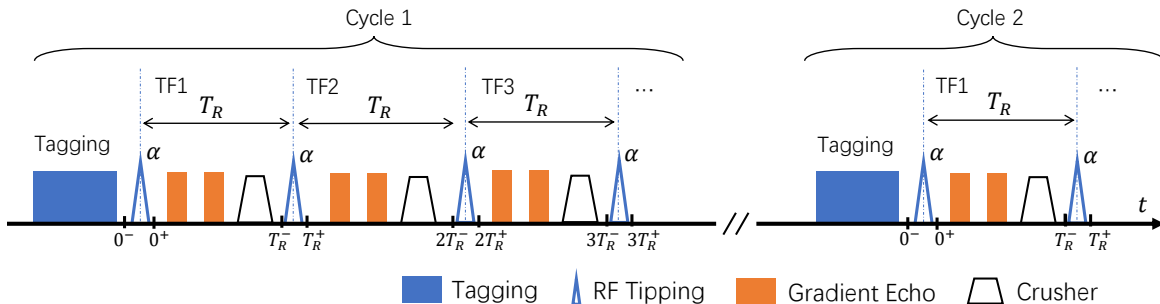


Figure 1. tMRI imaging sequence. “TF” stands for time-frame.

Recent advances in deep learning-based registration techniques have given rise to a new approach that directly employs *unsupervised* registration algorithms on *raw* tagged-MRI, using normalized cross-correlation (NCC) as a similarity objective.^{14,15} The underlying assumption is that the preservation of brightness constancy may not be imperative, provided that the model is equipped with appropriate image similarity objectives, such as NCC. This notion is similar to the premise of inter-modality registration tasks, where the intensity profile of the image pair does not necessarily exhibit a clear correlation or relationship.

This inspires us to assess the effectiveness of deep registration methods with diverse similarity objectives when dealing with tag fading. It also raises the question of whether harmonic phase-based techniques are becoming outdated in the deep learning (DL) era. In this study, we systematically compare the HARP-based and raw tag-based approaches using simulated tagged data undergoing a known motion and a real motionless phantom; therefore, in both cases the motion is known. Our analysis provides insights on how tag fading influences motion and strain estimation, and how different similarity objectives impact results. On a broader scale, this work reveals caveats and limitations of various similarity losses in registration tasks where the image intensity changes over time. Such scenarios can be found in pre- and post-intervention images and in the evolution of an injected contrast agent with patient motion.

The contributions of this work are summarized as follows: **(1)** We develop a mathematical model to capture the phenomenon of tag fading, factoring in the *interplay* of T_1 relaxation and transition to the steady state. **(2)** We evaluate and analyze the impact of widely-used similarity losses in training DL registration on tMRI. Simulated images and a real phantom scan are used to quantify the error of motion and strain, which are essential outputs in biomechanical studies.

2. METHOD

For our analysis, we have selected the classic 1:1 SPAMM²⁰ tagging sequence, which is shown in Fig. 1. The illustration demonstrates the process, wherein each tagging step is followed by a series of imaging sequences. During each T_R interval, the spin system is tipped by α and multiple line segments in k -space are captured using gradient echoes. To prepare for the next T_R interval, a crusher gradient is applied to dephase the magnetization in the transverse plane. The “tagging-imaging” cycle is repeated until sufficient k -space coverage is achieved. We denote the magnetization along the z -axis as M_z . We ignore the subtlety that the lines in k -space are acquired with varying amplitudes during T_2^* decay. Consequently, the amplitude of taglines at the n^{th} repetition time T_R are proportional to $M_z(x, nT_R^-)$, which can be iteratively represented in terms of $M_z(x, (n-1)T_R^-)$, given an initial condition, as

$$M_z(x, nT_R^-) = M_z(x, (n-1)T_R^+) \cdot e^{-\frac{T_R}{T_1}} + M_0 \left(1 - e^{-\frac{T_R}{T_1}}\right) \quad (1)$$

$$= M_z(x, (n-1)T_R^-) \cos(\alpha) \cdot e^{-\frac{T_R}{T_1}} + M_0 \left(1 - e^{-\frac{T_R}{T_1}}\right) \quad (2)$$

$$M_z(x, 0^-) = M_0 \cos(\gamma G_x \tau x) . \quad (3)$$

Equation 1 applies the T_1 -relaxation model. Equation 2 illustrates the application of the RF tipping with the tip angle α . Equation 3 represents the cosine pattern of magnetization that is introduced into the tissue immediately

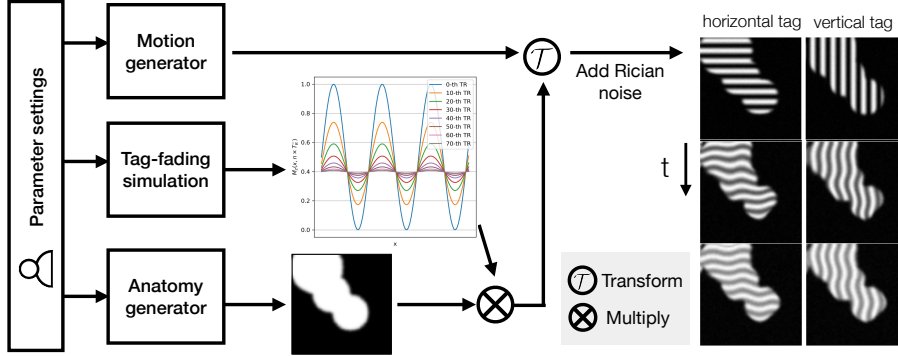


Figure 2. Simulation pipeline.

after the tagging process. In these equations, x denotes spatial location, M_0 the equilibrium magnetization magnitude, γ the gyromagnetic ratio, and G_x the x-direction magnetic gradient. With this tag-fading model, we can simulate 1:1 SPAMM tMRI sequences.

Simulation In this section, we simulate a dataset for DL model training and evaluation. Shown in Fig. 2, the simulation pipeline is composed of: the motion generator, the tag-fading simulation, and the anatomy generator. The motion generator creates an elastic deformation field that mimics tissue motion, while the tag-fading simulation manages the amplitude of tags at each time point, governed by Eqns. 1 through 3. The anatomy generator produces random disks whose union represents the anatomy being imaged. The process of tagging tissue is modeled as the multiplication of anatomy with tag patterns. The images are then warped by the generated deformation field to simulate deformed tag lines. Rician noise (with $\sigma = 0.02$) is subsequently added.

Registration framework Typically, DL-based registration frameworks aim to learn a function $\phi = g_\theta(F, M)$, where ϕ is the transformation used to align the fixed image F and the moving image M . The function g is parameterized by the learnable parameters θ . These parameters are learned by optimizing a generalized objective:

$$\hat{\theta} = \arg \min_{\theta} \mathcal{L}_{\text{sim}}(F, M \circ g_\theta(F, M)) + \lambda \mathcal{L}_{\text{smooth}}(g_\theta(F, M)). \quad (4)$$

\mathcal{L}_{sim} encourages image similarity between the fixed, F , and warped moving, M , images. $\mathcal{L}_{\text{smooth}}$ imposes a smoothness constraint on the transformation and λ weights the relative impact of two terms.

It is not feasible to evaluate all DL-based registration architectures. Instead, we selected the popular convolutional neural network (CNN)-based registration architecture, VoxelMorph,²¹ as our network backbone. We considered various similarity losses, including mean square error (MSE), normalized cross correlation²²(NCC), mutual information²³ (MI), structural similarity index²⁴ (SSIM), normalized gradient fields²⁵ (NGF), and modality independent neighborhood descriptor^{26,27} (MIND). These choices encompass the most widely-used similarity measurements for both mono- and multi-modal registration. For a comprehensive discussion on the characteristics of the various similarity losses, we refer readers to the review.²⁸ We encourage the spatial smoothness of the displacement \mathbf{u} , with the smoothness loss $\mathcal{L}_{\text{smooth}} = \sum_{\mathbf{x}} \|\nabla \mathbf{u}(\mathbf{x})\|^2$.

3. EXPERIMENTS

Materials & Training Details We generated a dataset comprising 1,000 “movies” through simulation (Fig. 2), where each movie consists of 40 time frames, each of size 96×96 . Each movie exhibits a unique anatomy, which subsequently undergoes random elastic deformation. During the generation process, the values for T_1 and T_R are randomly sampled from the intervals $[800, 1000]$ ms and $[15, 25]$ ms, respectively. The RF tip angle is set to $\alpha = 15^\circ$. The tag period is determined as 10% of the image dimension, i.e., 9.6 pixels. We split the data samples into training, validation, and testing datasets using a 6:2:2 ratio, respectively. In addition, we acquired a real tMRI sequence consisting of 78 time frames by scanning a static cylindrical gel phantom filled with Sylgard 527 in a 1:1 ratio, with material properties that emulate human brain tissue. Note that this phantom has no motion and the ground truth is zero deformation. This real phantom data is exclusively reserved for testing.

Table 1. Quantitative Results. The **best**, **second best**, and **worst** performing method in each column are highlighted. Wilcoxon signed-rank tests were conducted on pairs (labeled by brackets on the right) for all four columns, with * indicating statistical significance with $p < 0.01$ (with Bonferroni correction).

Input	Method	\mathcal{L}_{sim}	Synthetic Cases		Real Phantom	
			EPE ↓	MPS ⁹⁵ ↓	EPE ↓	MPS ⁹⁵ ↓
Raw tMRI	SyN	MSE	0.69 ± 0.25	0.35 ± 0.16	2.23 ± 1.02	0.88 ± 0.41
		CC	0.48 ± 0.25	0.16 ± 0.07	0.45 ± 0.16	0.17 ± 0.09
		MI	0.48 ± 0.25	0.13 ± 0.03	0.35 ± 0.10	0.08 ± 0.03
	VoxelMorph	MSE	1.49 ± 1.02	4.32 ± 4.59	0.55 ± 0.25	0.75 ± 0.37
		NCC	0.37 ± 0.13	0.50 ± 0.22	0.18 ± 0.04	0.19 ± 0.03
		MI	0.42 ± 0.18	0.31 ± 0.10	0.27 ± 0.14	0.42 ± 0.24
		MIND	0.83 ± 0.04	1.30 ± 0.09	0.20 ± 0.05	0.40 ± 0.08
		NGF	0.60 ± 0.10	0.63 ± 0.02	0.24 ± 0.04	0.21 ± 0.02
		SSIM	0.48 ± 0.17	0.72 ± 0.30	0.24 ± 0.06	0.29 ± 0.07
	Sinusoidal-transformed HARP (sHARP)	SyN	MSE	0.38 ± 0.28	0.12 ± 0.11	0.28 ± 0.16
CC			0.37 ± 0.29	0.12 ± 0.11	0.19 ± 0.07	0.21 ± 0.08
MI			0.38 ± 0.22	0.07 ± 0.04	0.42 ± 0.31	0.10 ± 0.08
VoxelMorph		MSE	0.32 ± 0.19	0.25 ± 0.17	0.07 ± 0.02	0.06 ± 0.01
		NCC	0.26 ± 0.10	0.14 ± 0.09	0.07 ± 0.03	0.05 ± 0.01

To facilitate a fair comparison, we independently searched for the optimal hyperparameters for each choice of \mathcal{L}_{sim} using a Bayesian optimizer,²⁹ which has proven to be a more effective strategy than grid search. For instance, we searched for the bin size and Parzen window size for MI, the window size for NCC, and the illumination, contrast, and structural factors for SSIM. The weight λ for $\mathcal{L}_{\text{smooth}}$ was also searched. Given that the anatomical masks of the simulated images are available, we employed the Dice coefficient between the fixed and warped moving masks as the metric during the hyperparameter search. An alternative option is to employ End-Point Error (EPE) as the metric, given the availability of ground truth for synthetic deformation. However, in practical scenarios, pixel-wise ground truth is typically unavailable, making EPE an impractical performance indicator for the selection of hyperparameters. During both training and evaluation, we used the first frame as the fixed image, and sampled moving images from all the subsequent frames. We modified the initial convolutional layer’s input channels to accommodate both raw vertical and horizontal-tagged images, as well as sinusoidal-transformed HARP (sHARP) images,¹³ which is a variant of traditional HARP. The sHARP effectively eliminates discontinuities in phase images, thereby facilitating seamless end-to-end training.

Evaluation metrics Given a sequence of tagged images, we create registration pairs by selecting the first image as the fixed image and pairing it with each subsequent image as the moving image. Registration accuracy is assessed using the End Point Error (EPE), which measures the magnitude of deviation between the estimated and ground truth displacement vector fields. We evaluate the impact on strain computation by calculating the 95th percentile error of the maximum principle strain (MPS⁹⁵) for each static test pair, which quantifies erroneous strain measurements. For instance, a MPS⁹⁵ value of 0.07 signifies that 5% of the tissue undergoes length stretching of at least 7%. Evaluation on each registration pair yields a EPE and MPS⁹⁵.

Results We evaluate and compare the performance of the raw-based and HARP-based approaches under various selections of \mathcal{L}_{sim} , as well as SyN²² with various similarity metrics, all of which are summarized in Table 1. Generally, the HARP-based input outperforms the raw tMRI input in terms of EPE and MPS⁹⁵. Specifically, the “raw + MSE” method attempts to match the absolute profile of the faded tag pattern, which often leads to the creation of illusory motion. NCC performs relatively better with the raw tMRI since it captures the correlation of a local intensity profile (within a window), making it less sensitive to changes in absolute intensity. However, it still generates errors that are statistically significantly higher than those produced when using HARP-based images as input. The overall best performance is achieved when using the HARP-based input trained with NCC loss. The harmonic phase, being a material property, spans the range $[-\pi, \pi)$. Ideally, a perfect estimation would be achievable through matching the *absolute* phase value under MSE. However, our observations indicate that NCC slightly outperforms MSE in both EPE and MPS⁹⁵.

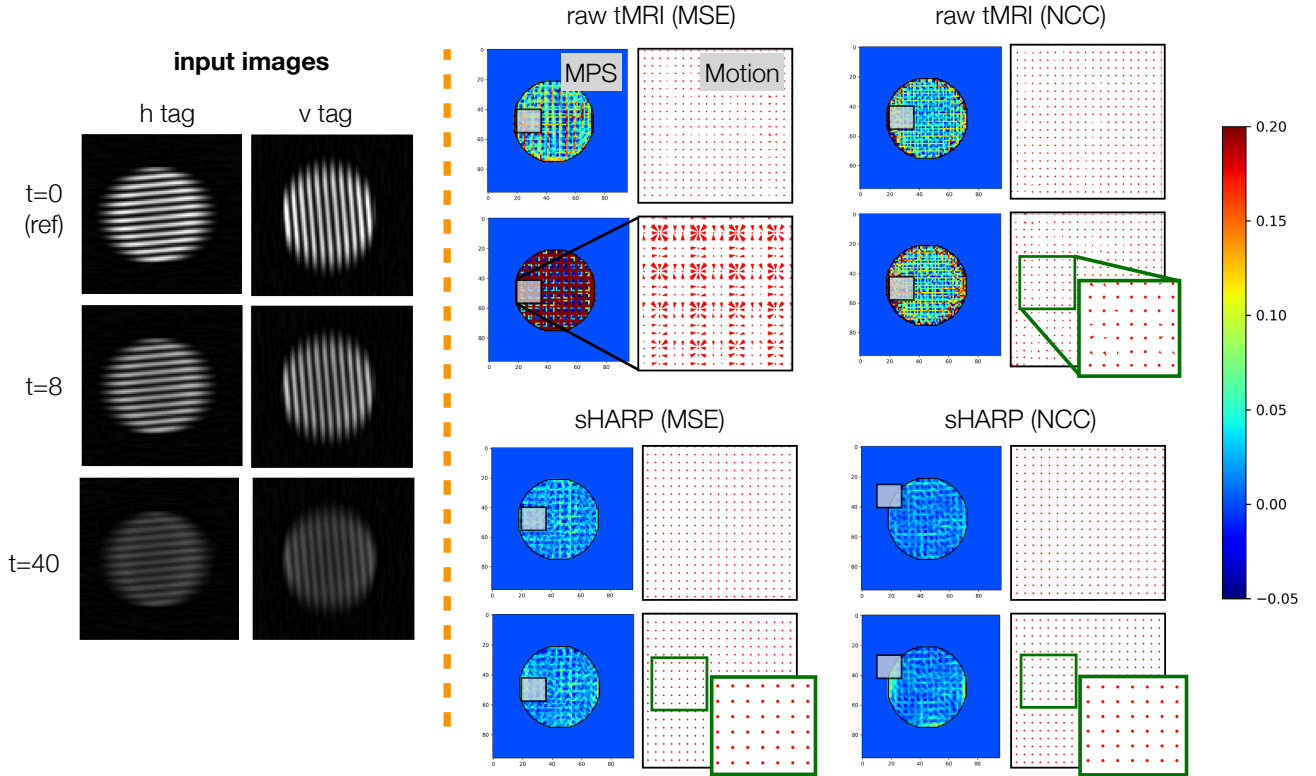


Figure 3. Qualitative results on real motionless data. Left panel shows horizontal (h-tag) and vertical (v-tag) tagging for three timeframes. Right panel shows the color-coded MPS⁹⁵ map and zoomed-in motion field of four methods. The first and second row show the registration results of ref-to-8th and ref-to-40th frame.

4. CONCLUSION

In this study, we constructed a mathematical model of MRI tagging to depict the phenomenon of tag fading, accounting for the interplay between T_1 relaxation and the progression toward steady-state during repeated imaging pulses, an aspect overlooked in previous research. We also take note of the recent trend in DL that uses raw tMRI as an input for motion or strain estimation. We perform a comparative analysis using Harmonic Phase (HARP) images versus raw tMRI as inputs for DL-based registration techniques. Our findings indicate that HARP-based input methods are less prone to generate false motion or strain when tag fading is present.

For future work, we intend to delve into deep similarity metric learning,^{30,31} which have shown promise in inter-modality image registration and are presumed to be robust against the challenges posed by tag fading. Although our current research is limited to SPAMM sequences, the potential of Complementary-SPAMM (CSPAMM) sequences to enhance tag contrast and mitigate tag fading cannot be ignored, despite their longer acquisition times. Current study of tag-fading dynamics could inform enhancements to the SPAMM sequence, aiming to achieve CSPAMM-level contrast while retaining rapid acquisition times.

Acknowledgments

This work was supported in part by the NIH through the National Institute of Neurological Disorders and Stroke (NINDS) grant U01-NS112120 (PI: P.V. Bayly) and the National Institute on Deafness and Other Communication Disorders (NIDCD) grant R01-DC018511 (PI: J. Woo). The opinions and assertions expressed herein are those of the authors and do not reflect the official policy or position of the Uniformed Services University of the Health Sciences or the Department of Defense.

REFERENCES

- [1] Axel, L. and Dougherty, L., “Heart wall motion: improved method of spatial modulation of magnetization for MR imaging,” *Radiology* **172**(2), 349–350 (1989).
- [2] Axel, L. and Dougherty, L., “MR imaging of motion with spatial modulation of magnetization,” *Radiology* **171**(3), 841–845 (1989).
- [3] McVeigh, E. R., Prinzen, F. W., Wyman, B. T., Tsitlik, J. E., Halperin, H. R., and Hunter, W. C., “Imaging asynchronous mechanical activation of the paced heart with tagged MRI,” *Mag. Reson. Med.* **39**(4), 507–513 (1998).
- [4] Parthasarathy, V., Prince, J. L., Stone, M., Murano, E. Z., and NessAiver, M., “Measuring tongue motion from tagged cine-MRI using harmonic phase HARP processing,” *The Journal of the Acoustical Society of America* **121**(1), 491–504 (2007).
- [5] Knutsen, A. K., Magrath, E., McEntee, J. E., Xing, F., Prince, J. L., Bayly, P. V., Butman, J. A., and Pham, D. L., “Improved measurement of brain deformation during mild head acceleration using a novel tagged MRI sequence,” *Journal of Biomechanics* **47**(14), 3475–3481 (2014).
- [6] Kolipaka, A., Chatzimavroudis, G. P., White, R. D., Lieber, M. L., and Setser, R. M., “Relationship between the extent of non-viable myocardium and regional left ventricular function in chronic ischemic heart disease,” *Journal of Cardiovascular Magnetic Resonance* **7**(3), 573–579 (2005).
- [7] Ibrahim, E.-S. H., “Myocardial tagging by cardiovascular magnetic resonance: evolution of techniques–pulse sequences, analysis algorithms, and applications,” *Journal of Cardiovascular Magnetic Resonance* **13**(1), 1–40 (2011).
- [8] Xing, F., Stone, M., Goldsmith, T., Prince, J. L., El Fakhri, G., and Woo, J., “Atlas-based tongue muscle correlation analysis from tagged and high-resolution magnetic resonance imaging,” *Journal of Speech, Language, and Hearing Research* **62**(7), 2258–2269 (2019).
- [9] Gomez, A. D., Stone, M. L., Woo, J., Xing, F., and Prince, J. L., “Analysis of fiber strain in the human tongue during speech,” *Computer methods in Biomechanics and Biomedical Engineering* **23**(8), 312–322 (2020).
- [10] Shao, M., Xing, F., Carass, A., Liang, X., Zhuo, J., Stone, M., Woo, J., and Prince, J. L., “Analysis of tongue muscle strain during speech from multimodal magnetic resonance imaging,” *Journal of Speech, Language, and Hearing Research* **66**(2), 513–526 (2023).
- [11] Osman, N. F. and Prince, J. L., “Visualizing myocardial function using HARP MRI,” *Physics in Medicine & Biology* **45**(6), 1665 (2000).
- [12] Xing, F., Woo, J., Gomez, A. D., Pham, D. L., Bayly, P. V., Stone, M., and Prince, J. L., “Phase vector incompressible registration algorithm for motion estimation from tagged magnetic resonance images,” *IEEE TMI* **36**(10), 2116–2128 (2017).
- [13] Bian, Z., Xing, F., Yu, J., Shao, M., Liu, Y., Carass, A., Woo, J., and Prince, J. L., “DRIMET: Deep Registration-based 3D Incompressible Motion Estimation in Tagged-MRI with Application to the Tongue,” in [6th *International Conference on Medical Imaging with Deep Learning (MIDL 2023)*], (2023).
- [14] Ye, M., Kanski, M., Yang, D., Chang, Q., Yan, Z., Huang, Q., Axel, L., and Metaxas, D., “Deeptag: An unsupervised deep learning method for motion tracking on cardiac tagging magnetic resonance images,” in [CVPR], 7261–7271 (2021).
- [15] Ye, M., Yang, D., Huang, Q., Kanski, M., Axel, L., and Metaxas, D. N., “SequenceMorph: A Unified Unsupervised Learning Framework for Motion Tracking on Cardiac Image Sequences,” *IEEE Trans. Patt. Anal. Mach. Intell.* **45**(8), 10409–10426 (2023).
- [16] Bian, Z., Wei, S., Liu, Y., Chen, J., Zhuo, J., Xing, F., Woo, J., Carass, A., and Prince, J. L., “Momentamorph: Unsupervised spatial-temporal registration with momenta, shooting, and correction,” *arXiv preprint arXiv:2308.02949* (2023).
- [17] Osman, N. F., Kerwin, W. S., McVeigh, E. R., and Prince, J. L., “Cardiac motion tracking using CINE harmonic phase (HARP) magnetic resonance imaging,” *Mag. Reson. Med.* **42**(6), 1048–1060 (1999).
- [18] Osman, N. F., McVeigh, E. R., and Prince, J. L., “Imaging heart motion using harmonic phase MRI,” *IEEE TMI* **19**(3), 186–202 (2000).
- [19] Yu, J., Shao, M., Bian, Z., Liang, X., Zhuo, J., Stone, M., and Prince, J. L., “New starting point registration method for tagged mri tongue motion estimation,” in [Medical Imaging 2023: Image Processing], **12464**, 519–523, SPIE (2023).
- [20] Park, J., Metaxas, D., and Axel, L., “Analysis of left ventricular wall motion based on volumetric deformable models and MRI-SPAMM,” *Center for Human Modeling and Simulation*, 99 (1996).
- [21] Balakrishnan, G., Zhao, A., Sabuncu, M. R., Guttag, J., and Dalca, A. V., “Voxelmorph: a learning framework for deformable medical image registration,” *IEEE TMI* **38**(8), 1788–1800 (2019).
- [22] Avants, B. B., Epstein, C. L., Grossman, M., and Gee, J. C., “Symmetric diffeomorphic image registration with cross-correlation: evaluating automated labeling of elderly and neurodegenerative brain,” *Medical Image Analysis* **12**(1), 26–41 (2008).
- [23] Viola, P. and Wells III, W. M., “Alignment by maximization of mutual information,” *International Journal of Computer Vision* **24**(2), 137–154 (1997).

- [24] Wang, Z., Bovik, A. C., Sheikh, H. R., and Simoncelli, E. P., “Image quality assessment: from error visibility to structural similarity,” *IEEE Trans. Imag. Proc.* **13**(4), 600–612 (2004).
- [25] Haber, E. and Modersitzki, J., “Intensity gradient based registration and fusion of multi-modal images,” in [*9th International Conference on Medical Image Computing and Computer Assisted Intervention (MICCAI 2006)*], 726–733, Springer (2006).
- [26] Heinrich, M. P., Jenkinson, M., Bhushan, M., Matin, T., Gleeson, F. V., Brady, M., and Schnabel, J. A., “Mind: Modality independent neighbourhood descriptor for multi-modal deformable registration,” *Medical Image Analysis* **16**(7), 1423–1435 (2012).
- [27] Heinrich, M. P., Jenkinson, M., Papież, B. W., Brady, S. M., and Schnabel, J. A., “Towards realtime multimodal fusion for image-guided interventions using self-similarities,” in [*16th International Conference on Medical Image Computing and Computer Assisted Intervention (MICCAI 2013)*], 187–194, Springer (2013).
- [28] Chen, J., Liu, Y., Wei, S., Bian, Z., Subramanian, S., Carass, A., Prince, J. L., and Du, Y., “A survey on deep learning in medical image registration: New technologies, uncertainty, evaluation metrics, and beyond,” *arXiv preprint arXiv:2307.15615* (2023).
- [29] Ozaki, Y., Tanigaki, Y., Watanabe, S., and Onishi, M., “Multiobjective tree-structured parzen estimator for computationally expensive optimization problems,” in [*Proceedings of the 2020 genetic and evolutionary computation conference*], 533–541 (2020).
- [30] Czolbe, S., Krause, O., and Feragen, A., “Semantic similarity metrics for learned image registration,” in [*Medical Imaging with Deep Learning*], 105–118, PMLR (2021).
- [31] Ronchetti, M., Wein, W., Navab, N., Zettinig, O., and Prevost, R., “Disa: Differentiable similarity approximation for universal multimodal registration,” in [*International Conference on Medical Image Computing and Computer-Assisted Intervention*], 761–770, Springer (2023).